

Supplemental information

Three-Dimensional Large-Pore Covalent Organic Framework with stp Topology

Hui Li,¹ Jiehua Ding,¹ Xinyu Guan,¹ Fengqian Chen,¹ Cuiyan Li,¹ Liangkui Zhu,¹ Ming Xue,¹ Daqiang Yuan,² Valentin Valtchev,^{3,4} Yushan Yan,⁵ Shilun Qiu,¹ and Qianrong Fang^{1*}

¹*State Key Laboratory of Inorganic Synthesis and Preparative Chemistry,
Jilin University, Changchun 130012, P. R. China*

E-mail: qrfang@jlu.edu.cn

²*State Key Laboratory of Structural Chemistry, Fujian Institute of Research on the Structure of Matter, Chinese Academy of Sciences, Fuzhou, 350002 Fujian, P. R. China*

³*Qingdao Institute of Bioenergy and Bioprocess Technology, Chinese Academy of Sciences, 189 Songling Road, Laoshan District, Qingdao, Shandong 266101, P. R. China*

⁴*Normandie Université, ENSICAEN, UNICAEN, CNRS, Laboratoire Catalyse et Spectrochimie, 14000 Caen, France*

⁵*Department of Chemical and Biomolecular Engineering, Center for Catalytic Science and Technology, University of Delaware, Newark, DE 19716, USA*

Table of contents

Section S1	Materials and characterization	S3-S6
Section S2	SEM image	S7
Section S3	TEM image	S7
Section S4	FT-IR spectra	S8
Section S5	Solid-state ^{13}C NMR spectra	S9
Section S6	TGA curve	S9
Section S7	Nitrogen adsorption	S10-12
Section S8	Summary of pore sizes	S13-15
Section S9	Adsorption of Mb	S16-19
Section S10	Unit cell parameters and fractional atomic coordinates	S20-21
Section S11	References	S22-24

Section S1. Materials and characterization

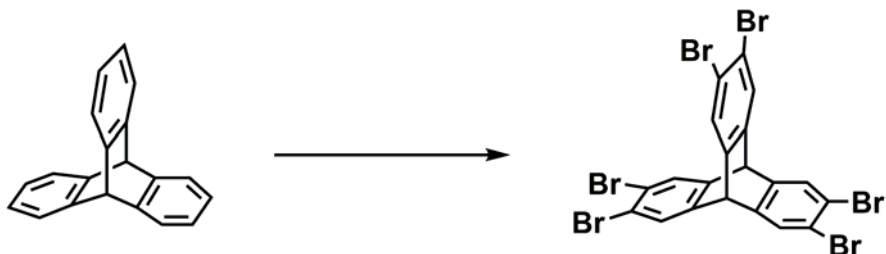
S1.1 Materials

All starting materials and solvents, unless otherwise noted, were obtained from J&K scientific LTD and used without further purification. All products were isolated and handled under nitrogen using either glovebox or Schlenk line techniques.

S1.2 Instruments

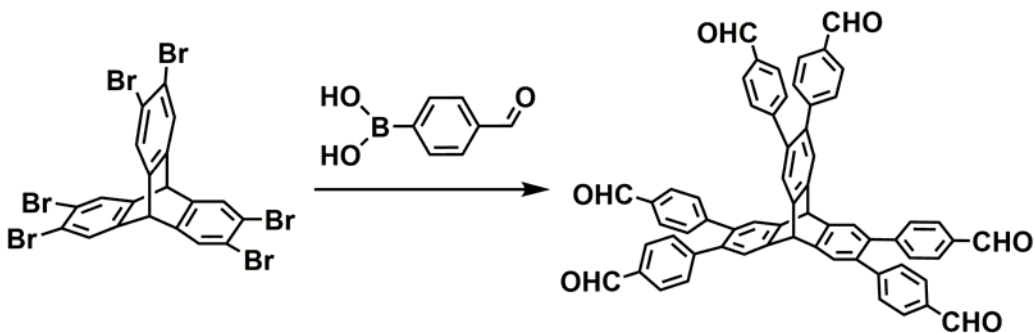
A Bruker AV-400 NMR spectrometer was applied to record the liquid ^1H NMR spectra. Solid-state ^{13}C NMR spectra were recorded on an AVIII 500 MHz solid-state NMR spectrometer. The FTIR spectra (KBr) were obtained using a SHIMADZU IRAffinity-1 Fourier transform infrared spectrophotometer. A SHIMADZU UV-2450 spectrophotometer was used for all absorbance measurements. Thermogravimetric analysis (TGA) was recorded on a SHIMADZU DTG-60 thermal analyzer under N_2 . The operational range of the instrument was from 30 °C to 800 °C at a heating rate of 10 °C min $^{-1}$ with N_2 flow rate of 30 mL min $^{-1}$. PXRD data were collected on a PANalytical B.V. Empyrean powder diffractometer using a Cu K α source ($\lambda = 1.5418 \text{ \AA}$) over the range of $2\theta = 2.0\text{--}40.0^\circ$ with a step size of 0.02° and 2 s per step. The sorption isotherm for N_2 was measured by using a Quantachrome Autosorb-IQ analyzer with ultra-high-purity gas (99.999% purity). To estimate pore size distributions for JUC-564, nonlocal density functional theory (NLDFT) was applied to analyze the N_2 isotherm on the basis of the model of $\text{N}_2@77\text{K}$ on carbon with slit pores and the method of non-negative regularization. For scanning electron microscopy (SEM) image, JEOL JSM-6700 scanning electron microscope was applied. Transmission electron microscopy (TEM) image was obtained on JEM-2100 transmission electron microscopy.

S1.3 Synthesis of 2,3,6,7,14,15-hexa(4'-formylphenyl)triptycene (HFPTP)¹



(1) Synthesis of 2,3,6,7,14,15-hexabromotriptycene

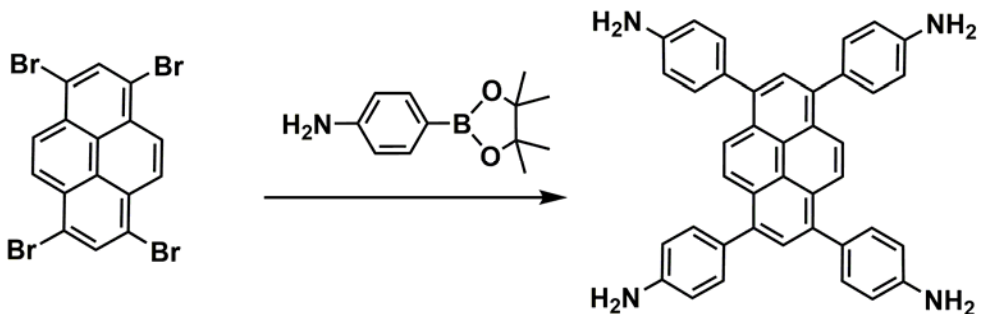
A mixture of triptycene (1.00 g, 3.9 mmol) and iron powder (80.0 mg, 1.45 mmol) was dissolved in 1,2-dichloroethane (60.0 mL). Bromine (1.32 mL, 25.7 mmol) was added slowly to the flask. Then the mixture was refluxing for 6h. After the reaction was cooled to 25 °C, the solvent and excess bromine were removed under reduced pressure. The residue was loaded on a short column (silica, CHCl₃) to give solid, which was recrystallized from CHCl₃ to give the pure product as colorless, needle-like crystals: (2.24 g, 3.1 mmol, 79%), m.p. > 350 °C; ¹H NMR (400 MHz, CDCl₃, 300 K): δ (ppm) 7.62 (s, 6 H), 5.24 (s, 2 H).



(2) Synthesis of HFPTP

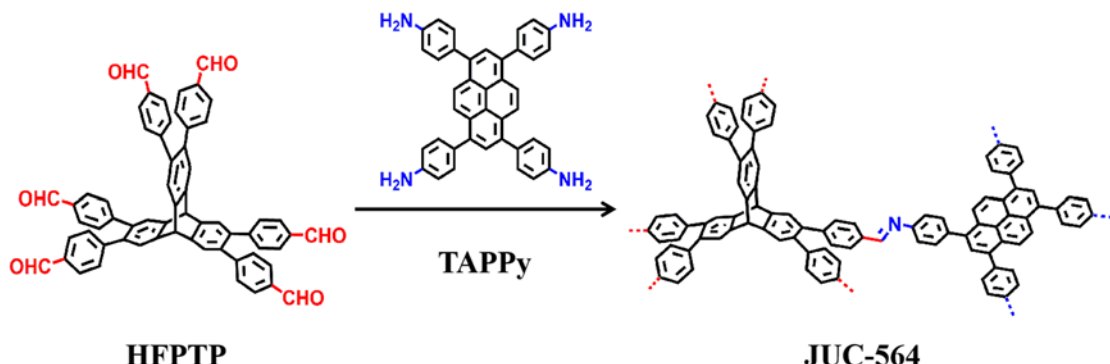
A mixture of 2,3,6,7,14,15-hexabromotriptycene (500.0 mg, 0.69 mmol), Cs₂CO₃ (2.90 g, 8.9 mmol.), Pd(PPh₃)₄ (0.24 g, 0.2 mmol) and (4-formylphenyl) boronic acid (1.33 g, 8.9 mmol) was dissolved in anhydrous THF (50.0 mL) and the mixture was heated and stirred at 65 °C under an argon atmosphere for 18 h. The solvent was removed under reduced pressure and the residue was dissolved in CH₂Cl₂ (100.0 mL). The crude product was washed sequentially with saturated NaHCO₃ (100.0 mL), deionized H₂O (100.0 mL) and brine (100.0 mL). The organic phase was dried with MgSO₄ and filtered. The solvent was removed in vacuo and the crude product was purified by column chromatography with silica gel (CH₂Cl₂/methanol, 25:1, v/v) and gave pure product as white crystals (426.0 mg, 0.48 mmol, 70 %), m.p. >300 °C. R_f = 0.55 (CH₂Cl₂/methanol, 20:1, v/v). ¹H NMR (400 MHz, CDCl₃): δ = 9.94 (s, 6 H), 7.70 (d, *J* = 8.0 Hz, 12 H), 7.61 (s, 6 H), 7.22 (d, *J* = 8.0 Hz, 12 H), 5.75 (s, 2 H) ppm. ¹³C NMR (100 MHz, CDCl₃): δ = 191.3, 146.5, 144.2, 136.7, 134.3, 130.1, 129.2, 125.8, 53.0 ppm.

S1.4 Synthesis of 1,3,6,8-tetra(4-aminophenyl)pyrene (TAPPY)²



A mixture of 1,3,6,8-tetrabromopyrene (1.48 g, 2.86 mmol), 4-aminophenylboronic acid pinacol ester (3.01 g, 13.7 mmol), K₂CO₃ (2.18 g, 15.7 mmol), and Pd(PPh₃)₄ (0.33 g, 0.29 mmol, 10 mol%) was dissolved in 32.0 mL 1,4-dioxane and 8.0 mL degassed H₂O and the mixture was heated and stirred at 115 °C under an argon atmosphere for 3 d. After cooling to room temperature, H₂O (50.0 mL) was added. The resulting precipitate was collected via filtration and was washed with H₂O (50.0 mL) and MeOH (100.0 mL). Recrystallization from 1,4-dioxane, followed by drying under high vacuum furnished the title compound, as a bright yellow powder (1.69 g, 2.56 mmol, 89 %).
¹H NMR (400 MHz, CDCl₃) δ (ppm): 8.13 (s, 4 H), 7.79 (s, 2 H), 7.34 (d, *J* = 8.4 Hz, 8 H), 6.77 (d, *J* = 8.5 Hz, 8 H), 5.30 (s, 8 H), 3.56 (s, 12 H, dioxane). ¹³C NMR (100 MHz, CDCl₃) δ: 148.2, 137.1, 131.0, 129.0, 127.6, 126.7, 126.1, 124.4, 113.9, 66.3 ppm.

S1.5 Synthesis of JUC-564



HFPTP (0.02 mmol, 18.0 mg) and TAPPY (0.03 mmol, 17.0 mg) were weighed into a Pyrex tube (volume: ca. 20.0 mL with a body length of 18.0 cm and neck length of 9.0 cm), and the mixture was added into 0.6 mL of mesitylene, 0.4 mL of dioxane and 0.2 mL of aqueous acetic acid (6 M). The Pyrex tube was flash frozen in a liquid nitrogen bath, evacuated to an internal pressure of ca. 19.0 mbar and flame-sealed, reducing the total length by ca. 10.0 cm. Upon warming to room

temperature, the tube was placed in an oven at 120 °C for 3 d. The resulting precipitate was filtered then exhaustively washed by Soxhlet extractions with dioxane for 48 h. The obtained powder was immersed in anhydrous acetone, and the solvent was exchanged with fresh acetone several times. The wet sample was then transferred to a super critical drier (Samdri-PTV-3D), in which the sample was washed six times with liquid CO₂, and exchanged with fresh CO₂ for six times with the interval of half an hour. The system was heated up to 45 °C to bring about the supercritical state of the CO₂, which was released after half an hour in very slow flow rate to ambient pressure. The sample was then transferred to vacuum chamber and evacuated to 20 mTorr under room temperature, yielding yellow powder (30.2 mg) for N₂ adsorption measurements. Anal. Cald for C₁₂₂H₇₁N₆: C: 90.40; H: 4.42; N: 5.18. Found: C: 91.40; H: 3.73; N: 4.87.

S1.6 Adsorption of Mb

The adsorption of a protein, myoglobin (Mb), in JUC-564 or COF-320 was monitored through UV-Vis spectrophotometry. Typically, 100.0 µg/mL of Mb from equine skeletal muscle (Sigma) was prepared in 20.0 mL 4-(2-hydroxyethyl)-1-piperazineethanesulfonic acid (HEPES) buffer added into 8.0 mg freshly activated COF powder and incubated at 37 °C. The supernatant was scanned at different time points to determine uptake of Mb by the decrease of the Soret band at 333 nm.

Section S2. SEM image



Figure S1. SEM image of as-synthesized JUC-564.

Section S3. TEM image

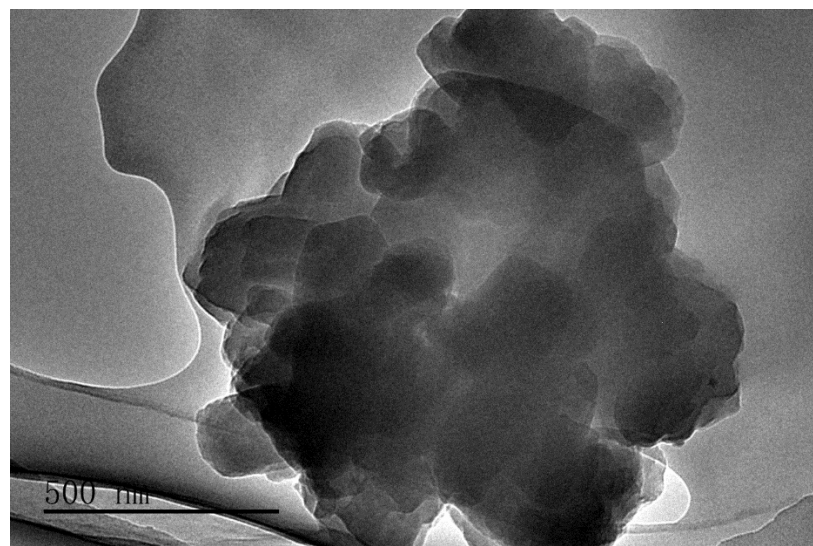
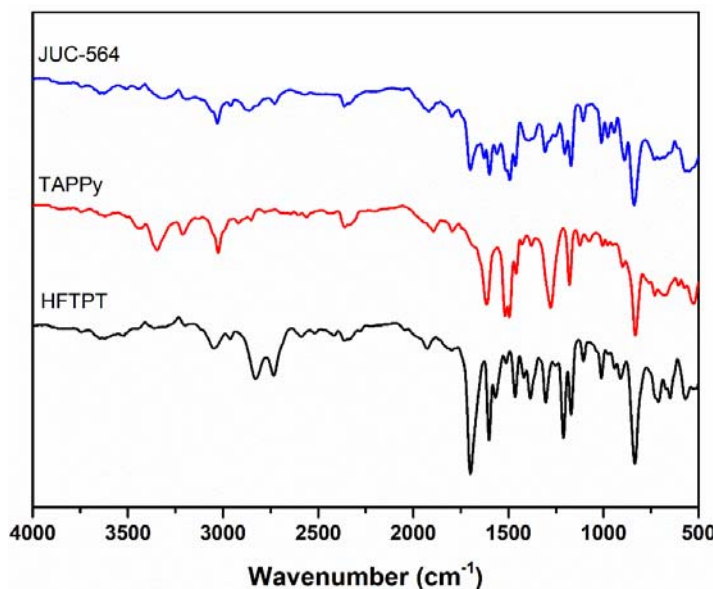


Figure S2. TEM image of as-synthesized JUC-564.

Section S4. FT-IR spectra



Peak (cm ⁻¹)	Assignment and notes for JUC-564
3312.52 (w)	N-H stretching of residual -NH ₂
3032.63 (w)	Aromatic C-H stretch
2954.73 (w)	Alkane C-H stretch from triptycene
2832.25 (w)	C-H stretching of residual aldehyde
2727.60 (w)	C-H stretching of residual aldehyde
2362.79	CO ₂
1700.21 (s)	C=O stretching of residual aldehyde
1627.87 (s)	Imine C=N stretching
1598.79 (s)	Aromatic ring stretching
1561.40 (m)	Aromatic ring stretching
1509.48 (s)	Aromatic ring stretching
1489.05 (s)	Aromatic ring stretching
1460.32 (m)	Aromatic ring stretching
1390.74 (br)	Alkane C-H deformation vibration from triptycene
1306.96 (m)	Aromatic ring stretching
1287.34 (vw)	Aromatic C-N stretching
1200.00 (s)	Imine C-C=N-C stretching.
1168.50 (m)	C-Ph breathing from triptycene
1015.14 (m)	Aromatic C-H in plane bending
980.53 (w)	Aromatic ring stretching
902.64 (w)	Aromatic C-H out of plane bending from triptycene
887.58 (m)	Aromatic C-H out of plane bending from pyrene
838.77 (s)	Aromatic C-H out of plane bending from phenylene

Figure S3. FT-IR spectra of HFPTP (black) and TAPPY (red), JUC-564 (blue).

Section S5. Solid-state ^{13}C NMR spectra

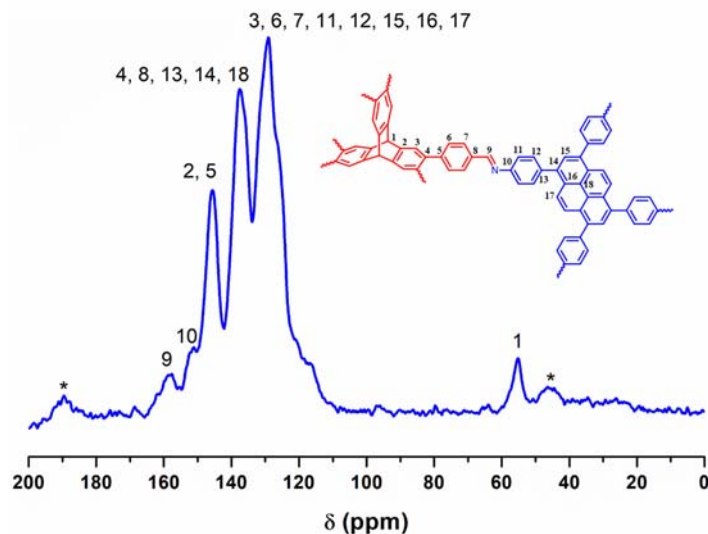


Figure S4. Solid state ^{13}C NMR of JUC-564. Asterisks (*) indicate peaks arising from spinning side bands.

Section S6. TGA curve

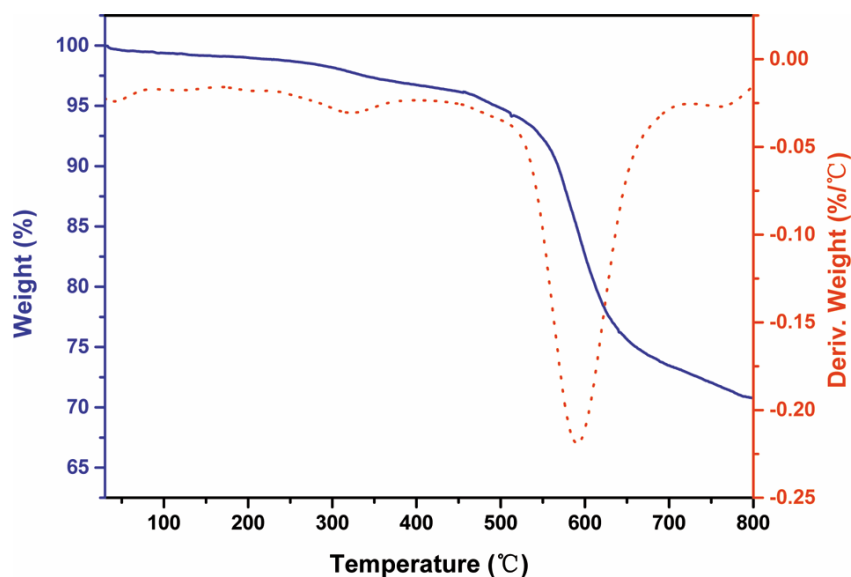


Figure S5. TGA (blue) and DTA (red) curves of JUC-564.

Section S7. Nitrogen adsorption

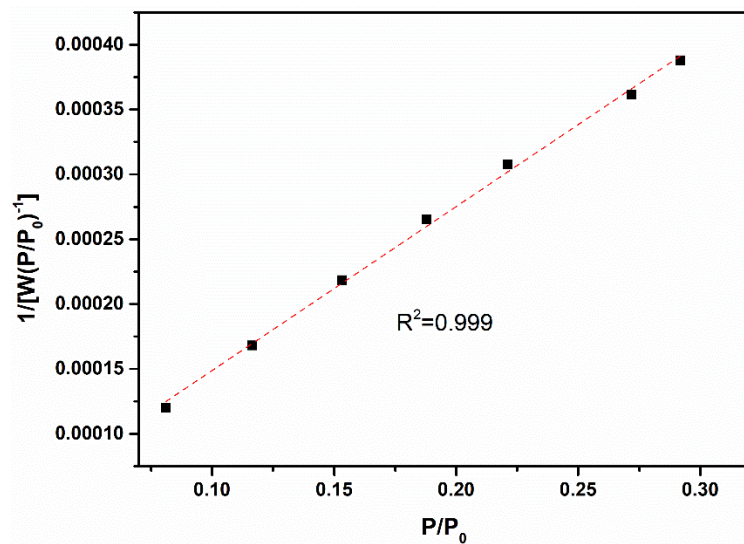


Figure S6. BET plot of JUC-564 calculated from N₂ adsorption isotherm at 77 K.

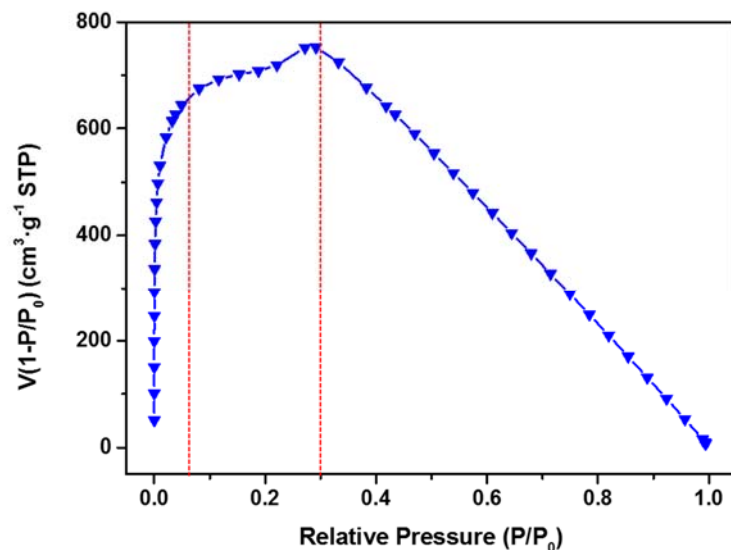


Figure S7. Rouquerol BET of JUC-564 calculated from N₂ adsorption isotherm at 77 K.

Table S1. All data points for the N₂ adsorption-desorption isotherm for JUC-564.

Relative Pressure (P/P ₀)	Quantity Adsorbed (cm ³ /g STP)
3.64661E-06	50.27078
1.50575E-05	100.7709
4.79381E-05	150.4086
0.000113399	199.4179
0.000237696	247.0849
0.000455306	292.527
0.000827742	336.7532
0.001532533	384.6217
0.002606183	427.2516
0.004149533	464.3601
0.006611402	501.1844
0.010356739	536.8796
0.02122637	595.8273
0.032472143	634.6012
0.038481791	651.2546
0.049299282	676.9428
0.08107324	734.3542
0.116402615	783.6721
0.153267674	828.6684
0.187910704	871.888
0.221254455	923.4808
0.271897533	1032.534
0.291895329	1062.431
0.332409477	1085.514
0.382675565	1096.738
0.418250662	1103.553
0.434509624	1106.861
0.469721971	1112.485
0.504391283	1117.879
0.539487157	1123.252
0.574490621	1128.653
0.609679373	1133.404
0.644581405	1138.143
0.679609723	1142.896
0.714604336	1147.702
0.749581371	1152.665
0.784601743	1157.784
0.819498286	1163.801
0.854503604	1170.707

0.889179388	1179.882
0.923691021	1194.009
0.956968859	1221.703
0.988968505	1309.268
0.992619542	1337.303
0.993352183	1347.089
0.994064695	1354.867
0.994521674	1362.22
0.982311456	1321.61
0.949598341	1248.992
0.906076178	1217.62
0.868134389	1203.413
0.832219547	1194.764
0.796828795	1188.276
0.780418274	1185.707
0.74534385	1181.028
0.710199863	1176.995
0.675331267	1173.121
0.640267903	1169.318
0.605306287	1165.568
0.570220962	1161.87
0.535198551	1157.877
0.500281284	1153.362
0.466388071	1141.881
0.429032255	1136.414
0.37680759	1128.244
0.360201752	1124.934
0.325374117	1117.145
0.29176756	1100.977
0.260308918	1059.514
0.218389174	968.4689
0.182547426	914.6015
0.153634076	878.8578
0.118366267	835.4444
0.082954941	784.6948
0.049789192	721.375

Section S8. Summary of pore sizes

Table S2. A summary of pore sizes in current reported 3D COFs.

RCSR code	Compound	Largest pore size (Å)	Reference
stp	JUC-564	43	this work
dia	COF-300	7.2	3
	COF-320	11.5	4
	MCOF-1	6.4	5
	PI-COF-4	13	6
	PI-COF-5	10	
	3D-OH-COF	13.1	7
	3D-COOH-COF	6.8	
	LZU-301	6.1	8
	3D-ionic-COF-1	8.6	9
	3D-ionic-COF-2	8.2	
	COF-DL229	14	10
	CCOF 5	7.4	11
	CCOF 6	7.4	
	3D-IL-COF-1	8.3	12
	3D-IL-COF-2	10.7	
	3D-IL-COF-3	12.4	
	SP-3D-COF-1	12	13
	SP-3D-COF-2	15	
	JUC-508	13	14
	JUC-509	12	
	COF 1	7.8	15
	COF 1-Zn	7.8	
	COF 2	7.8	
	COF 2-Zn	7.8	
	JUC-550	10.6	16
	JUC-551	14	
	JUC-552	22	
	JUC-525	6.2	17
	JUC-526	6.6	
	JUC-530	13.2	18
	JUC-531	16.1	
pts	3D-Py-COF	5.9	19
	3D-Por-COF	10.7	20
	3D-CuPor-COF	11.8	
	3D-TPE-COF	5.7	21
	COF-500-Cu	12.66	22
	3D-PdPor-COF	5.8	23

	3D-TPB-COF-H	5.6	24
	3D-TPB-COF-Me	5.2	
	3D-TPB-COF-F	5.2	
	JUC-518	15.4	25
	JUC-519	8.4	
	3D-BMTA-COF	8.5	26
ctn	COF-102	11.5	27
	COF-103	12.5	
	COF-202	11	28
	BF-COF-1	8.3	29
	BF-COF-2	8.1	
	DL-COF-1	13.6	30
	DL-COF-2	12.8	
bor	DBA-3D-COF 1	28	31
	Ni-DBA-3D-COF	26	
ffc	3D-ETTA-TFPB	17.3	32
	3D-ETTA-TFPA	14.9	
	COF-1	11.8	33
	COF-2	11.8	
rra	CD-COF	6.4	34
srs	SiCOF-5	-	35
ion	LZU-111	10.9	36

Table S3. A summary of BET surface areas and pore sizes in 3D imine-based COFs.

Compound	BET (m ² /g))	Largest pore size (Å)	Reference
JUC-564	3383	43	this work
COF-300	1360	7.2	3
COF-320	2400 (Langmuir)	11.5	4
3D-OH-COF	1077	13.1	7
3D-COOH-COF	540	6.8	
LZU-301	654	6.1	8
3D-ionic-COF-1	966	8.6	9
3D-ionic-COF-2	880	8.3	
COF-DL229	1762	14	10
CCOF 5	655	7.4	11
CCOF 6	613	7.4	
3D-IL-COF-1	517	8.3	12
3D-IL-COF-2	653	10.7	
3D-IL-COF-3	870	12.4	
SP-3D-COF 1	641	12	13
SP-3D-COF 2	1582	15	

JUC-508	1513	13	14
JUC-509	1443	12	
COF 1	666	7.8	15
COF 2	701	7.8	
COF 1-Zn	460	7.8	
COF 2-Zn	535	7.8	
JUC-550	846	10.6	16
JUC-551	1728	14	
JUC-552	3023	22	
JUC-525	372	6.2	17
JUC-526	386	6.6	
JUC-530	962	13.2	18
JUC-531	1579	16.1	
3D-Py-COF	1290	5.9	19
3D-Por-COF	1398	10.7	20
3D-CuPor-COF	1335	11.8	
COF-500-Cu	352	12.66	22
3D-PdPor-COF	1406	5.8	23
3D-TPB-COF-H	1050	5.6	24
3D-TPB-COF-Me	950	5.2	
3D-TPB-COF-F	850	5.2	
JUC-518	3018	15.4	25
JUC-519	1513	8.4	
3D-BMTA-COF	1650	8.5	26
BF-COF-1	730	8.3	29
BF-COF-2	680	8.1	
3D-ETTA-TFPB	1174	17.3	32
3D-ETTA-TFPA	1202	14.9	
LZU-111	2120	10.9	36

Section S9. Adsorption of Mb

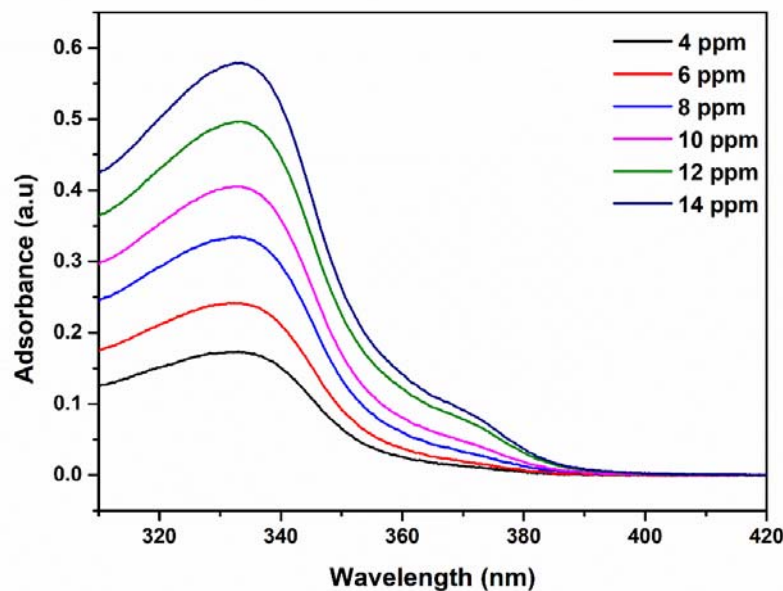


Figure S8. UV-vis spectrum for Mb with different concentrations, which is the data for a standard curve.

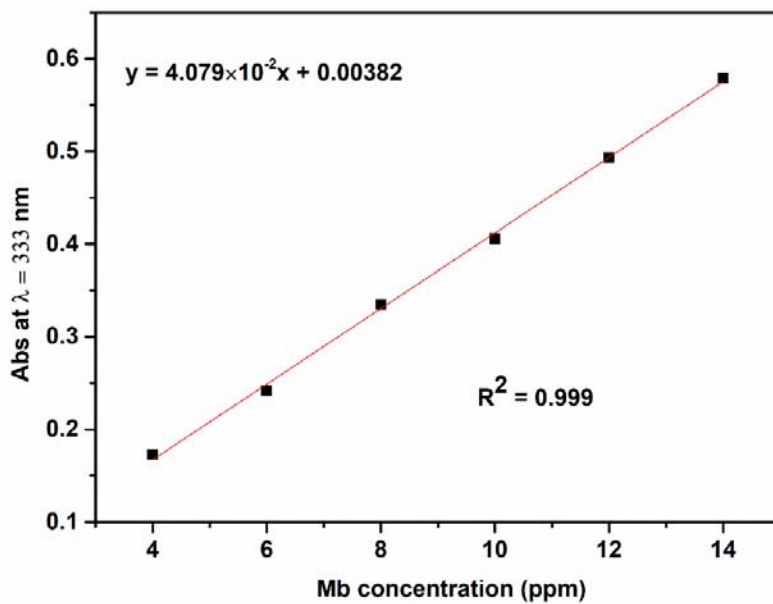


Figure S9. The standard curve of Mb.

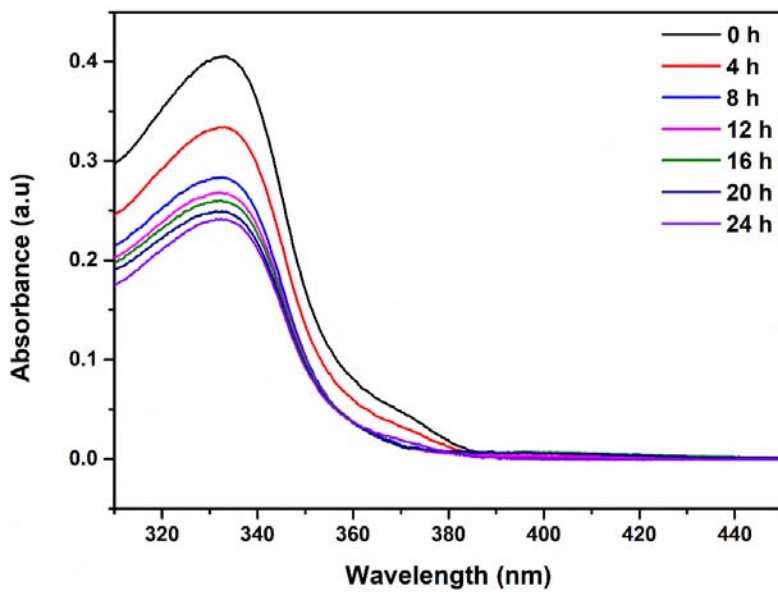


Figure S10. UV-vis spectrum of the supernatant solution containing Mb above JUC-564.

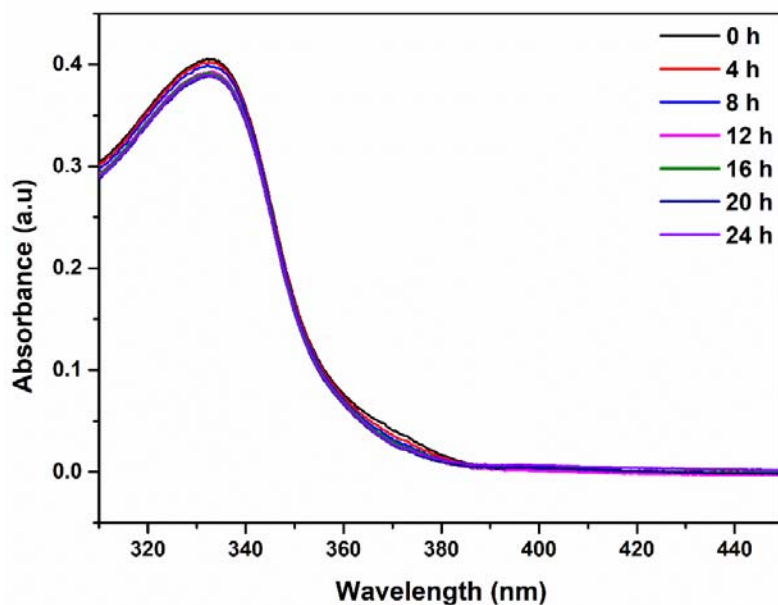


Figure S11. UV-vis spectrum of the supernatant solution containing Mb above COF-320.

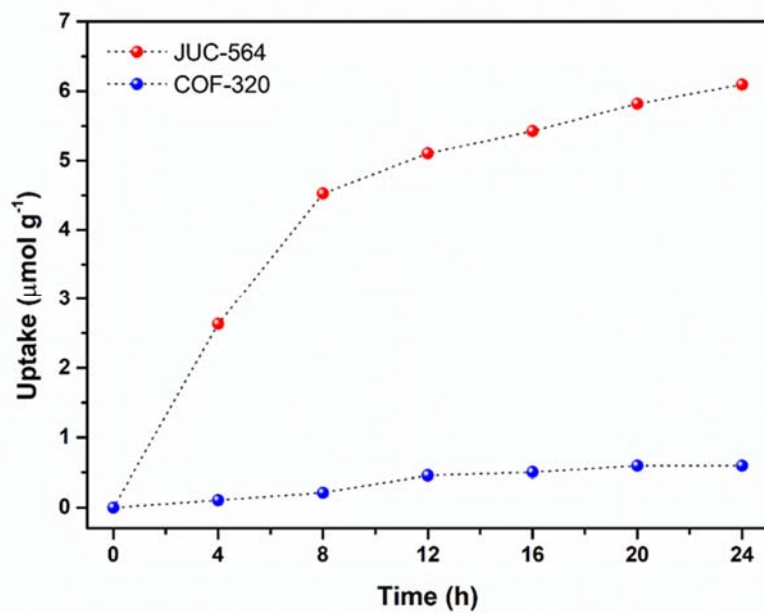


Figure S12. A comparison of uptake of Mb vs time in JUC-564 and COF-320, in which a rate constant of $0.57 \mu\text{mol} (\text{g h})^{-1}$ before 8 h for JUC-564 was obtained.

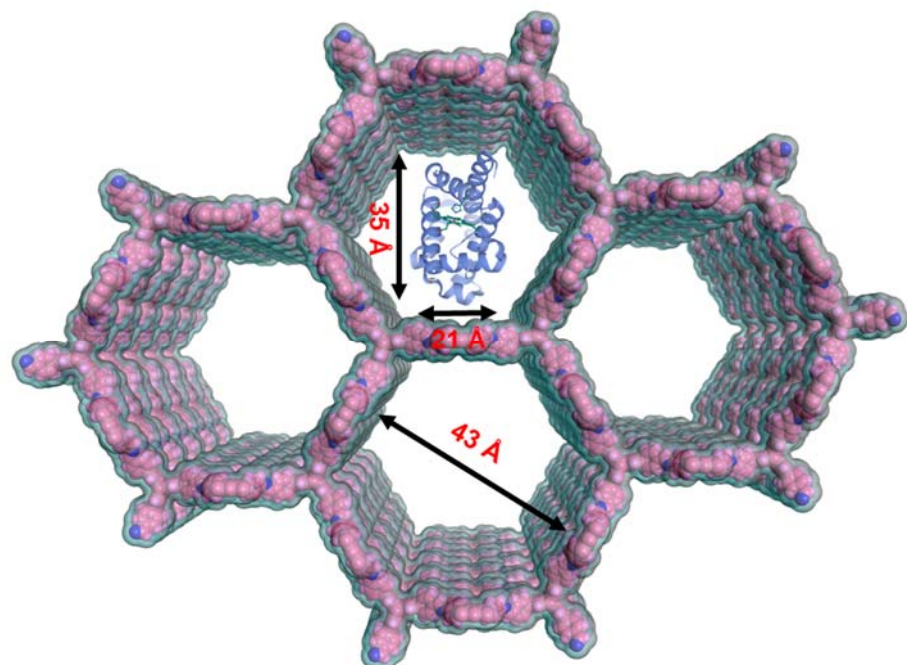


Figure S13. A schematic visualization of Mb in pores of JUC-564.

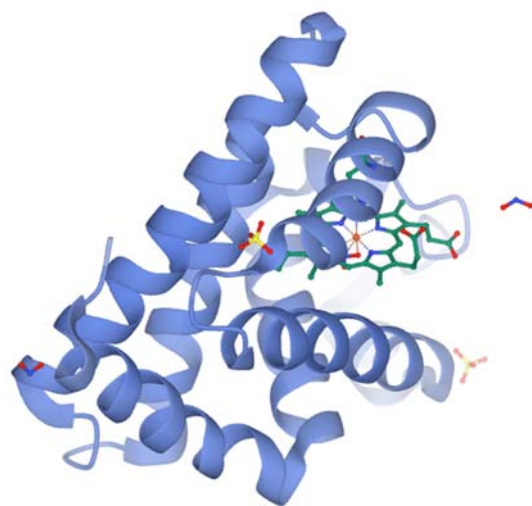


Figure S14. The structure of Mb (PDB 3LR7) with calculated molecular sizes of $44 \text{ \AA} \times 35 \text{ \AA} \times 21 \text{ \AA}$.³⁷

Section S10: Unit cell parameters and fractional atomic coordinates

Table S4. Unit cell parameters and fractional atomic coordinates for JUC-564 calculated based on the **stp** net.

Space group		<i>P</i> 6/m	
Calculated unit cell		$a = b = 52.7911 \text{ \AA}$, $c = 20.4794 \text{ \AA}$, $\alpha = \beta = 90^\circ$, $\gamma = 120^\circ$	
Measured unit cell		$a = b = 52.8112 \text{ \AA}$, $c = 20.4914 \text{ \AA}$, $\alpha = \beta = 90^\circ$, $\gamma = 120^\circ$	
Pawley refinement		$R_p = 2.93\%$, $R_{wp} = 4.43\%$	
atoms	x	y	z
C1	0.40079	0.62437	0.57193
C2	0.43096	0.64208	0.58159
C3	0.44645	0.6315	0.61658
C4	0.43194	0.60315	0.64284
C5	0.4016	0.58549	0.6333
C6	0.38616	0.59607	0.59808
C7	0.44875	0.59256	0.68008
N8	0.43566	0.56715	0.7085
C9	0.43212	0.5312	0.78795
C10	0.44951	0.55444	0.74599
C11	0.47957	0.56395	0.74086
C12	0.49193	0.55083	0.77855
C13	0.47456	0.52814	0.8219
C14	0.4445	0.51815	0.82575
C15	0.48803	0.51486	0.93072
C16	0.4877	0.5143	0.86163
C17	0.38444	0.63541	0.53465
C18	0.36804	0.64535	0.56905
C19	0.4773	0.53034	0.96604
C20	0.35199	0.65531	0.53458
H21	0.44247	0.66408	0.56209
H22	0.46978	0.64552	0.6234
H23	0.38981	0.56353	0.65292
H24	0.36283	0.5822	0.59098
H25	0.47211	0.60685	0.68493
H26	0.4089	0.52334	0.7917
H27	0.49355	0.5811	0.70737
H28	0.51508	0.55844	0.77418
H29	0.43068	0.50029	0.85808
H30	0.36776	0.6453	0.62191
H31	0.46904	0.54288	0.94156

C32	0.5	0.5	0.82852
C33	0.5	0.5	0.03467
C34	0.33333	0.66667	0.43428
H35	0.5	0.5	0.22278
H36	0.33333	0.66667	0.62033

Section S11. References

- (1) Moylan, C.; Rogers, L.; Shaker, Y. M.; Davis, M.; Eckhardt, H.-G.; Eckert, R.; Ryan, A. A.; Senge, M. O. Preparation of Tri- and Hexasubstituted Triptycene Synthons by Transition Metal Catalyzed Cross-Coupling Reactions for Post-Modifications: Preparation of Tri- and Hexasubstituted Triptycene Synthons. *Eur. J. Org. Chem.* **2016**, *1*, 185.
- (2) Bessinger, D.; Ascherl, L.; Auras, F.; Bein, T. Spectrally Switchable Photodetection with Near-Infrared-Absorbing Covalent Organic Frameworks. *J. Am. Chem. Soc.* **2017**, *139*, 12035.
- (3) Uribe-Romo, F. J.; Hunt, J. R.; Furukawa, H.; Klöck, C.; O'Keeffe, M.; Yaghi, O. M. A Crystalline Imine-Linked 3-D Porous Covalent Organic Framework. *J. Am. Chem. Soc.* **2009**, *131*, 4570.
- (4) Zhang, Y.; Su, J.; Furukawa, H.; Yun, Y.; Gándara, F.; Duong, A.; Zou, X.; Yaghi, O. M. Single-Crystal Structure of a Covalent Organic Framework. *J. Am. Chem. Soc.* **2013**, *135*, 16336.
- (5) Ma, H.; Ren, H.; Meng, S.; Yan, Z.; Zhao, H.; Sun, F.; Zhu, G. A 3D Microporous Covalent Organic Framework with Exceedingly High C₃H₈/CH₄ and C₂ Hydrocarbon/CH₄ Selectivity. *Chem. Commun.* **2013**, *49*, 9773.
- (6) Fang, Q.; Wang, J.H.; Gu, S.; Kaspar, R. B.; Zhuang, Z.; Zheng, J.; Guo, H.X.; Qiu, S.; Yan, Y. 3D Porous Crystalline Polyimide Covalent Organic Frameworks for Drug Delivery. *J. Am. Chem. Soc.* **2015**, *137*, 8352.
- (7) Lu, Q. Y.; Ma, Y. C.; Li, H.; Guan, X. Y.; Yusran, Y.; Xue, M.; Fang, Q. R.; Yan, Y. S.; Qiu, S. L.; Valtchev, V. Postsynthetic Functionalization of Three-Dimensional Covalent Organic Frameworks for Selective Extraction of Lanthanide Ions. *Angew. Chem. Int. Ed.* **2018**, *57*, 6042.
- (8) Ma, Y. X.; Li, Z. J.; Wei, L.; Ding, S. Y.; Zhang, Y. B.; Wang, W. A Dynamic Three-Dimensional Covalent Organic Framework. *J. Am. Chem. Soc.* **2017**, *139*, 4995.
- (9) Li, Z.; Li, H.; Guan, X.; Tang, J.; Yusran, Y.; Li, Z.; Xue, M.; Fang, Q.; Yan, Y.; Valtchev, V.; Qiu, S. Three-Dimensional Ionic Covalent Organic Frameworks for Rapid, Reversible, and Selective Ion Exchange. *J. Am. Chem. Soc.* **2017**, *139*, 17771.
- (10) Wang, C.; Wang, Y.; Ge, R.; Song, X.D.; Xing, X.; Jiang, Q.K.; Lu, H.; Hao, C.; Guo, X.W.; Gao, Y.N.; Jiang, DL. A 3D Covalent Organic Framework with Exceptionally High Iodine Capture Capability. *Chem. - Eur. J.* **2018**, *24*, 585.
- (11) Han, X.; Huang, J.; Yuan, C.; Liu, Y.; Cui, Y. Chiral 3D Covalent Organic Frameworks for High Performance Liquid Chromatographic Enantioseparation. *J. Am. Chem. Soc.* **2018**, *140*, 892.
- (12) Guan, X.; Ma, Y.; Li, H.; Yusran, Y.; Xue, M.; Fang, Q.; Yan, Y.; Valtchev, V.; Qiu, S. Fast, Ambient Temperature and Pressure Ionothermal Synthesis of Three-Dimensional Covalent Organic Frameworks. *J. Am. Chem. Soc.* **2018**, *140*, 4494.

- (13) Wu, C.; Liu, Y.; Liu, H.; Duan, C.; Pan, Q.; Zhu, J.; Hu, F.; Ma, X.; Jiu, T.; Li, Z.; Zhao, Y. Highly Conjugated Three-Dimensional Covalent Organic Frameworks Based on Spirobifluorene for Perovskite Solar Cell Enhancement. *J. Am. Chem. Soc.* **2018**, *140*, 10016.
- (14) Yan, S.; Guan, X.; Li, H.; Li, D.; Xue, M.; Yan, Y.; Valtchev, V.; Qiu, S.; Fang, Q. Three-Dimensional Salphen-Based Covalent–Organic Frameworks as Catalytic Antioxidants. *J. Am. Chem. Soc.* **2019**, *141*, 2920.
- (15) Huang, J.; Han, X.; Yang, S.; Cao, Y.; Yuan, C.; Liu, Y.; Wang, J.; Cui, Y. Microporous 3D Covalent Organic Frameworks for Liquid Chromatographic Separation of Xylene Isomers and Ethylbenzene. *J. Am. Chem. Soc.* **2019**, *141*, 8996.
- (16) Wang, Y.; Liu, Y.; Li, H.; Guan, X.; Xue, M.; Yan, Y.; Valtchev, V.; Qiu, S.; Fang, Qianrong. Three-Dimensional Mesoporous Covalent Organic Frameworks through Steric Hindrance Engineering. *J. Am. Chem. Soc.* **2020**, *142*, 3736.
- (17) Yu, X.; Li, C.; Ma, Y.; Li, D.; Li, H.; Guan, X.; Yan, Y.; Valtchev, V.; Qiu, S.; Fang, Q. Crystalline, Porous, Covalent Polyoxometalate-Organic Frameworks for Lithium-Ion Batteries. *Micropor. Mesopor. Mat.* **2020**, *299*, 110105.
- (18) Ma, Y.; Wang, Y.; Li, H.; Guan, X.; Li, B.; Xue, M.; Yan, Y.; Valtchev, V.; Qiu, S.; Fang, Q. Three-Dimensional Chemically Stable Covalent Organic Frameworks via Hydrophobic Engineering. *Angew. Chem. Int. Ed.* **2020**, DOI: 10.1002/anie.202005277.
- (19) Lin, G.; Ding, H.; Yuan, D.; Wang, B.; Wang, C. A Pyrene-Based, Fluorescent Three-Dimensional Covalent Organic Framework. *J. Am. Chem. Soc.* **2016**, *138*, 3302.
- (20) Lin, G.; Ding, H.; Chen, R.; Peng, Z.; Wang, B.; Wang, C. 3D Porphyrin-Based Covalent Organic Frameworks. *J. Am. Chem. Soc.* **2017**, *139*, 8705.
- (21) Ding, H.; Li, J.; Xie, G.; Lin, G.; Chen, R.; Peng, Z.; Yang, C.; Wang, B.; Sun, J.; Wang, C. An AIEgen-Based 3D Covalent Organic Framework for White Light-Emitting Diodes. *Nat. Commun.* **2018**, *9*, 5234.
- (22) Liu, Y.; Diercks, C. S.; Ma, Y.; Lyu, H.; Zhu, C.; Alshimimri, S. A.; Alshihri, S.; Yaghi, O. M. 3D Covalent Organic Frameworks of Interlocking 1D Square Ribbons. *J. Am. Chem. Soc.* **2019**, *141*, 677.
- (23) Meng, Y.; Luo, Y.; Shi, J. L.; Ding, H.; Lang, X.; Chen, W.; Zheng, A.; Sun, J.; Wang, C. 2D and 3D Porphyrinic Covalent Organic Frameworks: The Influence of Dimensionality on Functionality. *Angew. Chem. Int. Ed.* **2020**, *59*, 3624.
- (24) Gao, C.; Li, J.; Yin, S.; Lin, G.; Ma, T.; Meng, Y.; Sun, J.; Wang, C. Isostructural Three-Dimensional Covalent Organic Frameworks. *Angew. Chem. Int. Ed.* **2019**, *58*, 9770.

- (25) Li, H.; Chang, J.; Li, S.; Guan, X.; Li, D.; Li, C.; Tang, L.; Xue, M.; Yan, Y.; Valtchev, V.; Qiu, S.; Fang, Q. Three-Dimensional Tetrathiafulvalene-Based Covalent Organic Frameworks for Tunable Electrical Conductivity. *J. Am. Chem. Soc.* **2019**, *141*, 13324.
- (26) Gao, C.; Li, J.; Yin, S.; Sun, J.; Wang, C. Twist Building Blocks from Planar to Tetrahedral for the Synthesis of Covalent Organic Frameworks. *J. Am. Chem. Soc.* **2020**, *142*, 3718.
- (27) El-Kaderi, H. M.; Hunt, J. R.; Mendoza-Cortes, J. L.; Cote, A. P.; Taylor, R. E.; O'Keeffe, M.; Yaghi, O. M. Designed Synthesis of 3D Covalent Organic Frameworks. *Science* **2007**, *316*, 268.
- (28) Hunt, J. R.; Doonan, C. J.; LeVangie, J. D.; Côté, A. P.; Yaghi, O. M. Reticular Synthesis of Covalent Organic Borosilicate Frameworks. *J. Am. Chem. Soc.* **2008**, *130*, 11872.
- (29) Fang, Q.; Gu, S.; Zheng, J.; Zhuang, Z.; Qiu, S.; Yan, Y. 3D Microporous Base-Functionalized Covalent Organic Frameworks for Size-Selective Catalysis. *Angew. Chem., Int. Ed.* **2014**, *53*, 2878.
- (30) Li, H.; Pan, Q.; Ma, Y.; Guan, X.; Xue, M.; Fang, Q.; Yan, Y.; Valtchev, V.; Qiu, S. Three-Dimensional Covalent Organic Frameworks with Dual Linkages for Bifunctional Cascade Catalysis. *J. Am. Chem. Soc.* **2016**, *138*, 14783.
- (31) Baldwin, L. A.; Crowe, J. W.; Pyles, D. A.; McGrier, P. L. Metalation of a Mesoporous Three-Dimensional Covalent Organic Framework. *J. Am. Chem. Soc.* **2016**, *138*, 15134.
- (32) Lan, Y.; Han, X.; Tong, M.; Huang, H.; Yang, Q.; Liu, D.; Zhao, X.; Zhong, C. Materials Genomics Methods for High-Throughput Construction of COFs and Targeted Synthesis. *Nat. Commun.* **2018**, *9*, 5274.
- (33) Kang, X.; Wu, X.; Han, X.; Yuan, C.; Liu, Y.; Cui, Y. Rational Synthesis of Interpenetrated 3D Covalent Organic Frameworks for Asymmetric Photocatalysis. *Chem. Sci.* **2020**, *11*, 1494.
- (34) Zhang, Y.; Duan, J.; Ma, D.; Li, P.; Li, S.; Li, H.; Zhou, J.; Ma, X.; Feng, X.; Wang, B. Three-Dimensional Anionic Cyclodextrin-Based Covalent Organic Frameworks. *Angew. Chem. Int. Ed.* **2017**, *56*, 16313.
- (35) Yahiaoui, O.; Fitch, A. N.; Hoffmann, F.; Fröba, M.; Thomas, A.; Roeser, J. 3D Anionic Silicate Covalent Organic Framework with srs Topology. *J. Am. Chem. Soc.* **2018**, *140*, 5330.
- (36) Ma, T.; Kapustin, E. A.; Yin, S. X.; Liang, L.; Zhou, Z.; Niu, J.; Li, L.-H.; Wang, Y.; Su, J.; Li, J.; Wang, X.; Wang, W. D.; Wang, W.; Sun, J.; Yaghi, O. M. Single-Crystal X-Ray Diffraction Structures of Covalent Organic Frameworks. *Science* **2018**, *361*, 48.
- (37) <https://www.rcsb.org/>.